Bulletin of the Seismological Society of America, Vol. 103, No. 5, pp. 2782–2796, October 2013, doi: 10.1785/0120120318

Probabilistic Analysis of the Korean Historical Earthquake Records

by Soung Eil Houng and Tae-Kyung Hong

Abstract Seismic-hazard assessment for earthquakes with long recurrence intervals requires long earthquake records. Historical records for seismic damage can complement instrumental earthquake records, which is particularly useful for low-seismicity regions. Uncertainty in epicenters and magnitudes, however, hinders the full use of historical earthquake records. A probabilistic method to determine the epicenters of historical events is presented. The epicenters of historical events are determined probabilistically considering the nature of seismicity such that the spatial distribution of seismicity is nearly stationary with time in a constant tectonic environment. The probabilities for historical events to have occurred at given locations can be calculated using an instrumental seismicity density function and a distance-dependent weighting function. A location is selected randomly from a set of candidate source locations, of which probabilities are greater than a given prescribed value. The epicentral seismic intensity for the determined source location is calculated using an intensity–distance relationship. The magnitude is determined using an intensity–magnitude relationship. The method is verified with analysis of seismic intensity data for earthquakes in California. The method is applied to an ~1900 year long Korean historical seismic record, and the magnitudes of historical earthquakes are estimated. The Gutenberg–Richter b values for the historical events are determined to be 0.73. It is observed that the northwestern and southern peninsula, and the southeastern offshore region have high seismic-hazard potentials.

Introduction

Assessment of seismic potential is crucial for the preparation of seismic-hazard mitigation (Frankel, 1995; Kagan and Jackson, 2000). Recurrence intervals of large earthquakes are important parameters for seismic-hazard assessment. In particular, maximum magnitudes provide the upper limits of the strength of earthquakes (e.g., Kijko and Graham, 1998; Koravos *et al.*, 2003; Thingbaijam and Nath, 2008), and are used for seismic design of national infrastructures including nuclear power plants (e.g., Klugel, 2005; Mueller, 2010; Ares and Fatehi, 2013). The maximum magnitudes are determined probabilistically based on observed seismicity for sufficient periods of time. However, it is difficult to judge whether sufficient seismicity was observed.

Stable intraplate regions, in particular, have low seismicity with relatively long recurrence intervals of earthquakes, resulting in a limited number of instrumental records. Also, the recurrence intervals and maximum magnitudes of great earthquakes in active tectonic regions are estimated with high uncertainty based on limited available instrumental records. For instance, the 11 March 2011 M 9.0 Tohoku-Oki earthquake occurred in a region where no earthquakes with magnitudes greater than M 8 have been recorded according to the instrumental earthquake records (Geller, 2011; Koketsu, 2012). However, high seismic risks have been expected according to historical and geological records (Goto, 2011). Thus, analysis based on long-period seismicity records is in high demand to account for the seismic hazards of earthquakes with long-recurrence intervals.

Seismic damage records in historical literature may be useful to complement instrumental seismicity records (Ambraseys, 1971). Historical seismic records are available in many countries, including China (Lee *et al.*, 1976), Japan (Usami, 1979), Mediterranean regions (Poirier and Taher, 1980), India (Rao and Rao, 1984), Europe (Rubbia, 2004), and Korea (Wada, 1912; Lee and Yang, 2006). Historical seismic records mostly describe seismic damage that is readily convertible to seismic intensity. Rigorous efforts have been made to assess seismic hazards based on historical records (e.g., Albarello and Mucciarelli, 2002; Miyazawa and Mori, 2009; Seo *et al.*, 2010). However, historical seismic records have inherent limitations for full use in seismic-hazard assessment due to their uncertainty in source parameters including event locations and magnitudes. Errors in epicentral locations may affect other source parameters including magnitudes. Thus, reasonable determination of epicentral locations of historical earthquakes is particularly important for seismic-hazard analysis based on historical records.

In conventional hazard analyses based on historical earthquakes, the places with the greatest damage in the historical record are assumed to be the epicentral locations

(Degasperi *et al.*, 1991; Lee and Yang, 2006). However, seismic-damage records in the historical literature are mainly for major cities or towns, whereas those were rarely kept for uninhabited remote regions such as offshore or mountainous areas. Further, the epicenters of offshore events can be mistakenly interpreted to be placed in coastal regions based on the spatial distribution of seismic intensities in major cities. Thus, the historical event locations can be skewed by the spatial distribution of major cities or towns. To reduce the inherent uncertainty in the epicentral locations of historical earthquakes, various approaches have been proposed (e.g., Degasperi *et al.*, 1991; Bakun and Wentworth, 1997).

In this paper, we introduce a method to determine the epicentral locations of historical earthquakes from historical seismic-damage records considering the instrumental seismicity. The magnitudes of historical events are estimated from recorded seismic intensities and the magnitude–intensity relationship. Properties of historical seismicity including the Gutenberg–Richter *b* value are discussed, which may be useful in seismic-hazard assessment for earthquakes with long recurrence intervals.

Tectonics and Seismicity

The Korean Peninsula is located at the far-eastern margin of the Eurasian plate. The Korean Peninsula experienced complex tectonic evolution with interactions between nonextended and extended continental crusts including continental collision and rifting (e.g., Chough *et al.*, 2000). The collision between the North and South China blocks formed the current shape of the Korean Peninsula during the late Permian to the Jurassic (e.g., Oh, 2006). Also, continental rifting during the Oligocene to the mid-Miocene opened the East Sea (Sea of Japan; Jolivet *et al.*, 1994).

The Korean Peninsula consists of three Precambrian massifs (Nangnim, Gyeonggi, and Yeongnam massifs), two Permo–Triassic orogenic belts (Imjingang and Okcheon fold belts; Ernst *et al.*, 2007), two Paleozoic sedimentary basins (Pyeongnam and Taebaeksan basins), and a Cretaceous Gyeongsang basin (Chough *et al.*, 2000; Oh, 2006; Fig. 1a). The major tectonic boundaries and faults were developed by major orogenic events during the late Paleozoic to the Mesozoic including the collision between North and South China blocks (Chough *et al.*, 2000).

A northeast-trending paleo-rifting system (Chugaryeong fault system) was formed in the central Korean Peninsula during the Holocene, displaying signatures of multiple volcanic activities (Lee *et al.*, 1983; Won *et al.*, 1990). However, the tectonic evolution responsible for formation of the Chugaryeong fault system remains unclear (e.g., Shibuya *et al.*, 1985; Ryu *et al.*, 2011). The crust of the Korean Peninsula presents typical characteristics of a continental crust. The crustal thicknesses are about 28–38 km (Chang and Baag, 2006; Hong *et al.*, 2008). The crustal thickness decreases abruptly across the east coast of the peninsula to the East Sea (Hong, 2010). The crustal thicknesses beneath the East Sea are 8.5–14 km (e.g., Hirata *et al.*, 1989; Kim *et al.*, 1998). The crustal structure beneath the East Sea displays a transitional structure between continental and oceanic crusts except in the central East Sea around the Japan basin

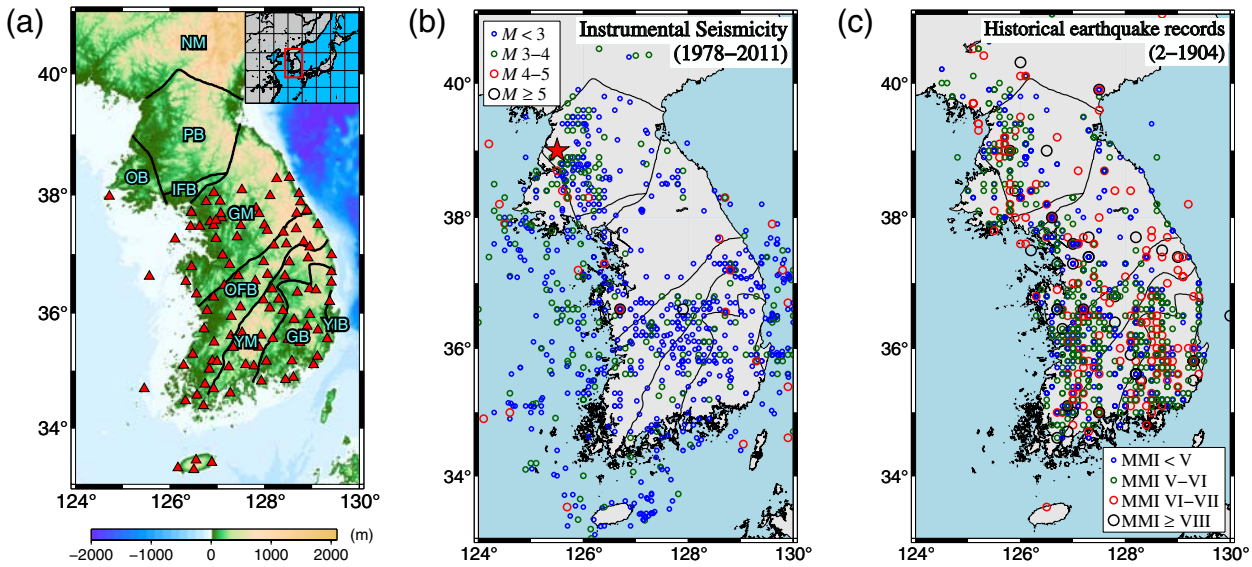

Figure 1. (a) Surface topography map with Korea Meteorological Administration (KMA) seismic stations; triangles, KMA seismic stations; thick lines, major geological provinces; NM, Nangnim massif; PB, Pyeongnam basin; OB, Ongjin basin; IFB, Imjingang fold belt; GM, Gyeonggi massif; OFB, Okcheon fold belt; YM, Yeongnam massif; GB, Gyeongsang basin; and YIB, Yeonil basin. (b) Instrumental seismicity around the Korean Peninsula during 1978–2011; star, epicenter of the largest earthquake on the Korean Peninsula since the introduction of modern seismographs. The event magnitude is M_S 6.5, and the event occurred on 19 March 1952 (Engdahl and Villasenor, 2002). (c) Locations with the greatest damage for historical earthquakes during 2–1904 A.D. The seismic damage is presented in the modified Mercalli intensity (MMI) scale. The color version of this figure is available only in the electronic edition.

in which an oceanic crust is present (Sato *et al.*, 2006; Hong, 2010; Kulinich and Valitov, 2011).

The Korean Peninsula belongs to an intraplate regime with low seismicity, and displays the typical characteristics of a stable nonextended continental crust. The focal depths of most events are less than 35 km (Hong and Choi, 2012). Seismicity is spatially scattered across the peninsula with clusters at northwestern and southern inland regions, and western and southeastern off-coast regions. Relatively low seismicity is observed in the central, northeastern, and northern inland regions (Fig. 1b). It is known that strike-slip earthquakes are dominant on the Korean Peninsula (Choi *et al.*, 2012; Hong and Choi, 2012). However, thrustal earthquakes caused by reverse activation of paleo-rifting structures occur in a region off the southeast coast (Hong and Kang, 2009; Choi *et al.*, 2012). The paleo-rifting structures are associated with the East Sea opening. Also, normal-faulting earthquakes are dominant around the northwestern offshore region where the paleo-collision belt between North and South China blocks is present (Hong and Choi, 2012).

The national earthquake monitoring program began in 1978. According to the earthquake catalog of the Korea Meteorological Administration (KMA), 949 earthquakes with magnitudes of 1.7–5.3 occurred on and around the Korean Peninsula during 1978–2011 (Fig. 1b). The instrumentally recorded earthquakes include five events with magnitudes greater than or equal to 5.0. Approximately nine earthquakes with magnitudes greater than or equal to 3.0 occur every year. It was reported that an M_S 6.5 earthquake occurred in 1952 on the northwestern peninsula, which is one of the highest seismicity regions on the Korean Peninsula (Engdahl and Villasenor, 2002; Fig. 1b).

The short history of instrumental seismic observation on the Korean Peninsula may not be enough for inference of earthquakes with long recurrence intervals of hundreds or thousands of years. Various historical literatures contain earthquake damage records for the Korean Peninsula during 2–1904 A.D. (Lee and Yang, 2006; Fig. 1c). The total number of historical earthquake records is 2185 with seismic intensities in the modified Mercalli intensity (MMI) scale of II–IX. The number of earthquakes with seismic intensities greater than or equal to VI is 240. Historical earthquake damage is observed in most regions of the Korean Peninsula. The number of earthquake damage records on the northeastern peninsula is relatively small compared with that on the southern and northwestern peninsula. This historical seismicity density is consistent with the instrumental seismicity density.

Theory

Probabilistic Determination of Historical Event Locations

The locations of cities or towns with the most severe damage have been assumed to be the epicenters of historical events in conventional studies (e.g., Lee *et al.*, 1976; Usami, 1979; Poirier and Taher, 1980; Lee and Yang, 2006), which may not be true in regions with sparse distribution of cities or towns. In this paper, a probabilistic method based on well-recorded instrumental seismicity is proposed for the determination of the epicenters of historical earthquakes.

Figure 1 presents the instrumental seismicity and the locations of cities or towns with the most severe damage by historical earthquakes. The most damaged locations in inland regions appear to be generally correlated with the instrumental seismicity. Also, it is observed that the most damaged locations are populated along the coasts of the peninsula. This may be because the reported seismic damage in coastal regions may be in part caused by offshore events.

The actual epicentral locations of historical earthquakes may be close to the cities or towns with the most severe damage relative to other cities or towns. Thus, the probability of finding the actual epicenter may decrease with its distance from the most damaged location. The probability of a historical event occurring at a certain location can be estimated considering both the instrumental seismicity density and the location with the most severe damage.

The probability of the ith historical event ($i = 1, 2, \ldots, N_{\text{he}}$) to have occurred at the jth discretized cell ($j = 1, 2, \ldots, N_c$), P_{ij}, is given by

$$P_{ij} = A \times C_j \times F_{ij}, \tag{1}$$

for which A is a normalization factor yielding $\sum_{j=1}^{N_c} P_{ij} = 1$, C_j is a normalized instrumental seismicity density at the jth cell, and F_{ij} is a weighting factor reflecting the distance from the presumed location of event i to the jth cell. Here note that the normalized instrumental seismicity density C_j and the weighting factor F_{ij} satisfy $\sum_{j=1}^{N_c} C_j = 1/B_{\max}$ and $\sum_{j=1}^{N_c} F_{ij} = 1$.

We define the instrumental seismicity density B_j to be

$$B_j = \frac{1}{N_{\text{ie}}} \frac{\sum_{k=1}^{N_c} (n_k \times G_{jk})}{\sum_{k=1}^{N_c} G_{jk}}, \tag{2}$$

in which N_{ie} is the number of instrumentally observed events, n_k is the number of instrumentally observed events in the kth cell, and G_{jk} is a Gaussian function centering on the jth cell. The Gaussian function smoothes the spatial distribution of instrumental seismicity density. The Gaussian function (G_{jk}) is given by

$$G_{jk} = \frac{1}{2\pi\sigma^2} \exp\left(\frac{-l_{jk}^2}{2\sigma^2}\right), \tag{3}$$

in which σ controls the spatial width of the function, and l_{jk} is the distance between jth and kth cells. The maximum value of B_j is defined to be $B_{\max}$:

$$B_{\max} = \max\{B_j, j = 1, 2, \ldots, N_c\}. \tag{4}$$

The normalized instrumental seismicity density C_j is calculated by

$$C_j = \frac{B_j}{B_{\max}}. \tag{5}$$

The weight factor F_{ij} presents a probability density function as a function of distance, which is given by

$$F_{ij} = \frac{K \times \exp(-K \times d_{ij})}{1 - \exp(-K \times d_{\max})}, \quad \text{for} \quad d_{ij} \le d_{\max},$$
$$= 0, \quad \text{for} \quad d_{ij} > d_{\max}, \tag{6}$$

for which d_{ij} is the distance from the presumed location of the historical event i to the jth cell, and K is a positive constant controlling the decay rate of the exponential function with distance. The integration of F_{ij} with distance up to $d_{\max}$ is given by 1, satisfying the nature of the weighting factor. The maximum distance $d_{\max}$ is determined by considering the spatial distribution of major cities or towns.

The probability of a historical event occurring at a discretized cell is calculated based on equation (1). The normalized probability P_{ij}^n is given by

$$P_{ij}^n = \frac{P_{ij}}{P_i^{\max}}, \tag{7}$$

in which $P_i^{\max}$ is the greatest probability in all cells. Cells with normalized probabilities greater than a prescribed value P_c are considered to be potential locations of the historical event. A location is selected randomly from the pool of candidate locations as a probable epicenter of the historical event. The number of candidate locations is affected by the prescribed value P_c implemented. When a large P_c is applied, cells with high probabilities are collected. Thus, the number of candidate locations decreases with increasing P_c.

When the instrumental seismicity density is uniform over the region (i.e., $C_j = 1$), the probability P_{ij} is mainly controlled by the distance-dependent weighting function F_{ij}. In this case, the highest probability is given to locations of cities with the most severe damage, and probabilities decrease with distance from the most damaged cities. Considering the instrumental seismicity density, the epicenters of historical earthquakes may be located in any places within distances of $d_{\max}$ from the most damaged cities. Thus, it is desirable that the prescribed level of probability P_c is determined to be sufficiently low enough to include all probable cells.

Magnitude Determination

The magnitudes of historical earthquakes are determined using the seismic intensities at the epicenters (Lee *et al.*, 1976; Usami, 1979; Lee and Yang, 2006). The epicentral seismic intensities are calculated from the recorded seismic intensities in certain cities or towns. The attenuation of seismic intensity as a function of distance in the Sino–Korean craton is given by (Lee and Kim, 2002)

$$I_0 = I + 1.75 \ln\left[1 + 0.59\left(\frac{l}{l_0} - 1\right)\right], \tag{8}$$

in which I_0 is the epicentral seismic intensity in the MMI scale, I is the MMI seismic intensity at a distance of l, and l_0 is the radius of the region with the epicentral seismic intensity of I_0 (Fig. 2). Parameter l_0 varies by 5.2, 6.5, and 9.3 km for I_0 less than or equal to VIII, IX, and X (Lee and Kim, 2002).

In this paper, the epicentral seismic intensities (I_0) are estimated from the reported seismic intensities at distant locations (I). For unique determination of epicentral seismic intensities, it is desirable to implement a single intensity–attenuation relationship. The average value of reference distances (l_0) is 7.0 km, which is implemented into the intensity–attenuation relationship in this paper. It is noteworthy that magnitudes may vary up to ±0.3 magnitude units for different l_0.

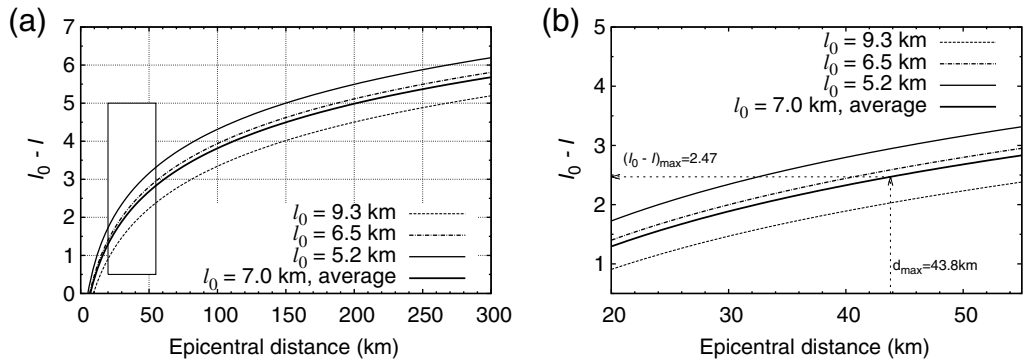

Figure 2. (a) Intensity I attenuation as a function of distance in the Sino–Korean craton for three reference distances (l_0 = 5.2, 6.5, and 9.3 km) that vary with the epicentral intensity I_0. (b) An enlarged graph for the range marked with a rectangle in (a). A representative intensity–attenuation curve is designed with implementation of the average value of three reference distances (l_0 = 7.0 km). The seismic intensity decreases by 2.47 at a distance of $d_{\max}$ (43.8 km) based on the reference intensity–attenuation curve.

The magnitudes of events are estimated from the epicentral seismic intensities. Several magnitude–intensity relationships have been proposed for the Korean Peninsula (e.g., Lee and Lee, 2003; Kim, 2012). A recent relationship that has been developed based on the refined seismicity information is applied (Kim, 2012):

$$M_L = 1.13 + 0.58I_0, \quad (9)$$

in which M_L is the local magnitude, and I_0 is the epicentral intensity. From equations (8) and (9), a combined relationship between the magnitude (M_L) and observed intensity (I) for $l_0 = 7.0$ km is given by

$$M_L = 0.58I + 1.02\ln(0.59l + 2.87) - 0.86, \quad (10)$$

in which l is the epicentral distance in km.

Data

The source information of 949 instrumentally recorded earthquakes during 1978–2011 is collected from the Korea Meteorological Administration and Korea Institute of Geoscience and Mineral Resources (KIGAM). The event magnitudes are 1.7–5.3. The seismic monitoring capability on the Korean Peninsula has kept increasing. The seismic stations of KMA are deployed densely and near uniformly over the southern Korean Peninsula as of December 2012 (Fig. 1a). The average interstation distance is 20.83 km.

The minimum magnitude M_{min} of an instrumental event catalog is estimated to ensure the completeness of records (e.g., Ogata and Katsura, 1993; Wiemer and Wyss, 2000; Woessner and Wiemer, 2005). The minimum magnitude is estimated using the Gutenberg–Richter magnitude–frequency relationship

$$\log N = a - b \times M, \quad (11)$$

in which M is magnitude, N is the annual number of events with magnitudes greater than M, and a and b are constants. Constants a and b are estimated using the maximum likelihood estimation method (Wiemer and Wyss, 2000). Residuals between observed and synthetic data are calculated for various lower bounds of magnitudes (Fig. 3a). Large residuals in low-magnitude ranges ($M < 2.0$) suggest incomplete event records in the catalog (Fig. 3a). Also, large residuals are observed at large magnitude ranges ($M > 4.0$) due to insufficient large-size events for stable estimation of the Gutenberg–Richter constants.

The residuals for minimum magnitudes M_{min} of 2.5–3.2 are less than 10%. In this paper, magnitude 2.5 is used as the minimum magnitude to include the maximum number of events, 642, enhancing the stability of the analysis. The b value is determined to be 0.81 for M_{min} of 2.5 (Fig. 3b). The spatial distribution of earthquakes with magnitudes greater than 2.5 is close to that of earthquakes with magnitudes greater than 3.2, suggesting that the collected seismicity displays complete spatial coverage. This observation is consistent with a previous paper reporting that the earthquakes with magnitudes greater than 2.3–2.7 are detected completely on the Korean Peninsula (Sheen and Shin, 2010).

The estimated b value is consistent with previous studies (Lee *et al.*, 2003; Seo *et al.*, 2010). Also, the estimated b value is consistent with typical b values in intraplate regions that are given by 0.7–1.3 (Okal and Sweet, 2007). The estimated b value and similar seismicity densities suggest that a 33 year long earthquake catalog may be sufficient for analysis of spatial variation of seismicity on the Korean Peninsula.

Historical earthquakes were recorded in various historical sources including Samgooksagi, Koryosa, and Choseonwangjosillog, which were listed by various studies (e.g., Wada, 1912; Lee and Yang, 2006). The seismic intensities and source information of historical events during

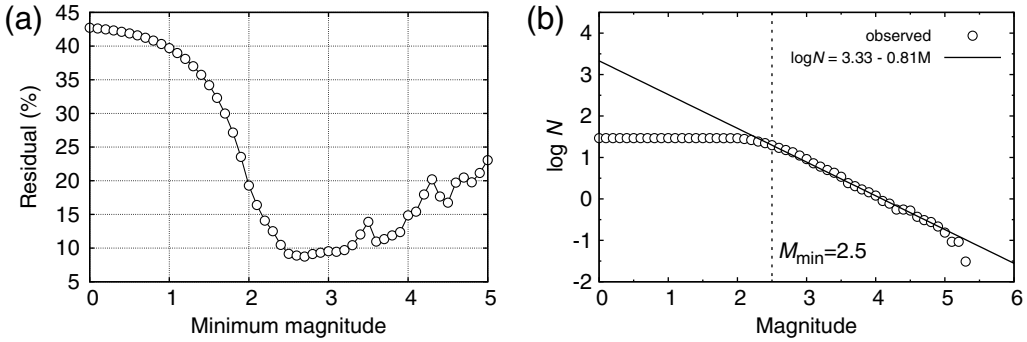

Figure 3. (a) Residuals between the observed magnitude–frequency data of instrumental seismicity and the theoretical variation as a function of the minimum magnitude (M_{min}). The residuals decrease with the increasing similarity between the observed data and theoretical variation. The residuals generally decrease with increasing minimum magnitude up to M_{min} of 2.7. The residuals vary significantly at $M_{min} > 3.2$, which may be associated with an insufficient number of data. Residuals are found to be less than 10% at M_{min} of 2.5–3.2. (b) Gutenberg–Richter magnitude (M)–frequency ($\log N$) relationship of instrumental seismicity for M_{min} 2.5, for which N is the annual number of events with magnitude equal to or greater than M. Open circles, observed instrumental magnitude data at a magnitude interval of 0.1; solid line, theoretical Gutenberg–Richter magnitude (M)–frequency ($\log N$) line. The Gutenberg–Richter a and b values are determined to be 3.33 and 0.81.

2–1904 A.D. are collected from Lee and Yang (2006). The number of earthquakes during the period of the Three Kingdoms is 56, earthquakes during the period of the Unified Silla is 33, earthquakes during the period of the Koryo dynasty is 158, and earthquakes during the period of the Choseon dynasty is 1938 (Fig. 4a).

The historical earthquake records during the Choseon dynasty comprise about 89% of the total historical earthquake records. Large-size events with seismic intensities of VIII to IX are recorded mostly in the periods before the Choseon dynasty. On the contrary, earthquakes with seismic intensities greater than IV were recorded well during the Choseon dynasty (Fig. 4). Thus, we use the historical earthquake records during the Choseon dynasty (1392–1904) for stable analysis of historical seismicity in this paper.

Process

Construction of Instrumental Seismicity Density Function

The normalized instrumental seismicity density C_j is calculated from equation (5). The normalized instrumental seismicity density is used as a probability mass function in determination of possible event locations. We set σ in equation (3) to be 20 km, which is sufficiently large to cover possible errors in the reported epicentral locations. Note that the event catalog presents event locations up to one decimal place, and $\sigma = 20$ km corresponds to approximately 2 times the precision limit of event locations in the event catalog. For discretized presentation of the instrumental density function, the study area in 30°–42° N and 120°–132° E is discretized by uniform cells with a size of $0.1° \times 0.1°$. The total number of cells N_c is 14,400. The events with magnitudes greater than $M_{\min}$ 2.5 are used in the analysis. The number of the events N_{ie} is 642.

A temporal and spatial window method is applied to identify possible foreshocks and aftershocks (Uhrhammer, 1986). Seventeen events are identified as plausible aftershocks of 13 mainshock events, presenting ~1.3 aftershocks per mainshock (Table 1). It is known that the magnitude differences between mainshocks and their largest aftershocks are ~1.2 magnitude units (Bath, 1965; Helmstetter and Sornette, 2003). However, the magnitudes of events identified as possible aftershocks are comparable to those of the mainshock events, suggesting that the identified events may not be actual aftershocks considering the magnitude differences.

The normalized seismicity densities C_j are compared between the original catalog and the declustered catalog to examine the influence of possible inclusion of aftershocks in the event catalog (Fig. 5). The seismicity density functions are observed to be similar between the two catalogs. This observation suggests that the possible inclusion of aftershocks would hardly cause changes in the determination of candidate locations of historical epicenters for low P_c. It is desirable to use the original full catalog in the analysis considering both the ambiguity in identification of aftershocks and their minimal influence on the constructed seismicity density function. Thus, the original full catalog is applied in this paper.

The east-central peninsula presents relatively low seismicity (Fig. 5a). Also, the seismicity densities present some localized high values. The highest seismicity is observed on the northwestern peninsula between 38°–40° N and 125°–126.5° E. The southeastern offshore, western offshore, and southern inland regions display high-seismicity densities. The high-seismicity regions coincide with regions of paleotectonic evolution. It was reported that the paleo-tectonic structures respond to the ambient stress fields, causing the occurrence of clustered earthquakes (Choi *et al.*, 2012; Hong and Choi, 2012).

Calculation of a Distance-Dependent Weighting Function

The historical records mainly describe seismic damage, which has an inherent lack of source information, such as event location. It is generally accepted that event epicenters may be located closer to the cities with the most severe

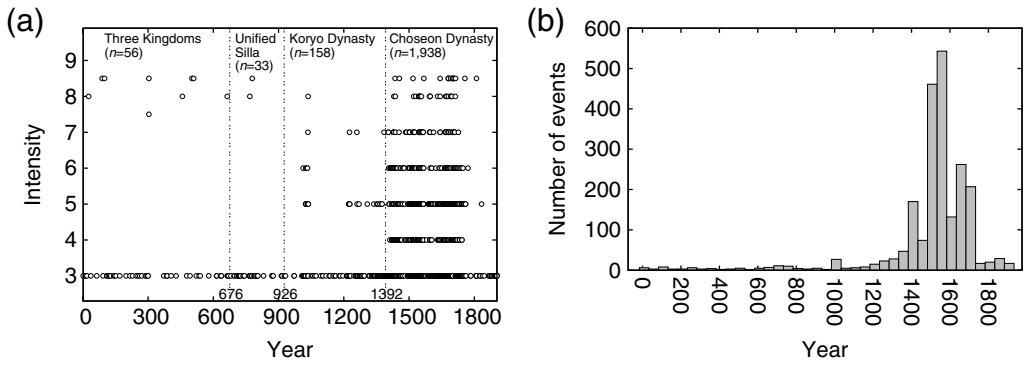

Figure 4. (a) Temporal distribution and seismic intensities of historical earthquakes during 2–1904 A.D. The number of events during the Three Kingdoms, Unified Silla, Koryo dynasty, and Choseon dynasty are 56, 33, 158, and 1938, respectively. The seismic intensities are distributed between 3 and 8.5. Small-to-large-sized historical earthquakes were well documented since 1392 (Choseon dynasty). (b) Histogram for the numbers of records for every 50 year time period. The numbers of records increase rapidly during the Choseon dynasty.

Table 1
Plausible Aftershocks Identified by a Spatial and Temporal Window Method

ID	Date (yyyy/mm/dd)	Time (UTC) (hh:mm:ss.s)	Latitude (°N)	Longitude (°E)	Magnitude (M_L)
M01	1980/12/01	04:29:57	40.7	127.2	3.5
A	1980/12/01	11:46:13	40.7	127.2	3.0
M02	1982/08/28	18:18:40	37.2	125.9	4.0
A	1982/08/29	06:29:13	37.1	125.9	3.3
M03	1982/08/29	06:34:01	37.1	126.0	3.5
A	1982/08/31	11:49:46	37.1	126.0	3.2
M04	1985/06/24	21:40:33	37.3	126.4	4.0
A	1985/06/24	22:29:32	37.3	126.4	3.8
A	1985/06/26	08:19:41	37.3	126.4	2.6
M05	1996/12/13	04:10:16.9	37.25	128.71	4.5
A	1996/12/13	04:27:08	37.3	128.8	3.0
A	1996/12/14	06:17:57	37.3	128.8	2.7
A	1996/12/15	07:20:40	37.2	128.8	2.5
M06	1997/05/09	12:40:07.1	35.29	126.32	3.2
A	1997/05/09	12:43:40	35.2	126.0	3.0
M07	1997/06/14	23:45:29.9	37.18	126.34	2.8
A	1997/06/15	03:46:37.5	37.18	126.35	2.7
M08	1999/03/14	11:20:30.6	37.88	130.93	3.2
A	1999/03/15	07:11:17	37.5	130.4	2.7
M09	1999/04/07	14:43:19	37.2	128.9	3.3
A	1999/04/07	15:40:23	37.2	128.9	2.9
A	1999/04/07	16:09:30	37.2	128.9	2.6
M10	2006/04/28	14:47:55.3	37.56	129.94	3.0
A	2006/04/28	14:54:57.6	37.54	129.93	2.5
M11	2008/11/11	12:20:54.7	38.51	125.66	3.0
A	2008/11/11	14:37:56.7	38.49	125.66	2.5
M12	2008/11/11	12:30:03.6	38.52	125.66	3.0
A	2008/11/11	14:37:56.7	38.49	125.66	2.5
M13	2009/05/01	22:58:28.0	36.56	128.71	4.0
A	2009/05/02	03:28:29.5	36.55	128.70	2.9

Mainshock events are indicated by M, and their aftershocks by A. The total number of mainshocks is 13. Single aftershock events are identified for most mainshock events, excepting three mainshock events.

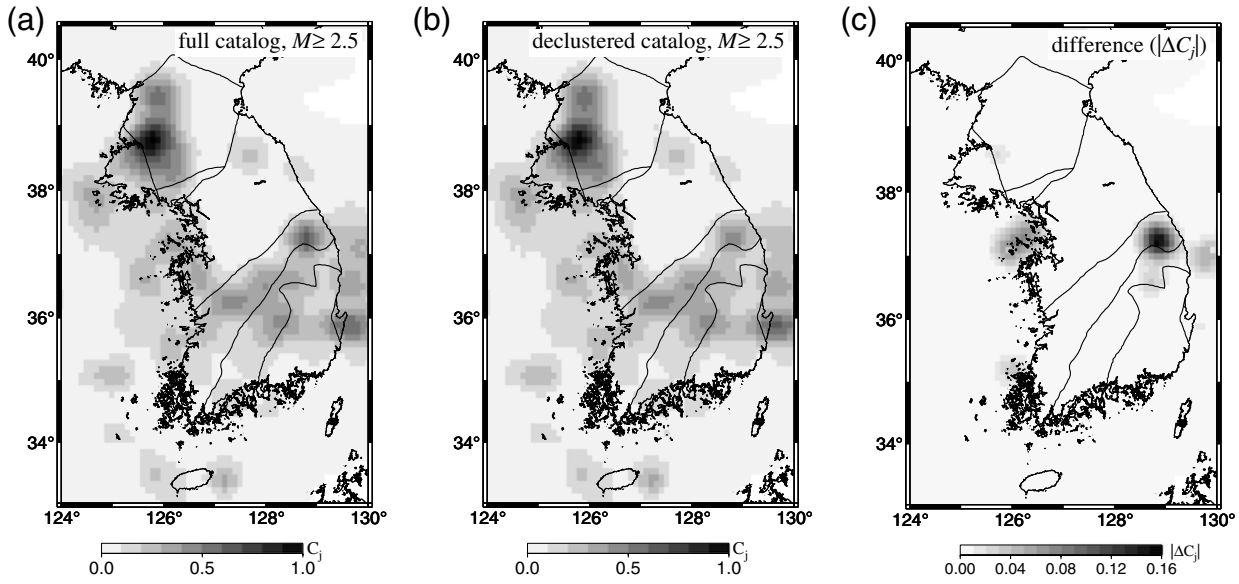

Figure 5. Instrumental seismicity densities C_j on and around the Korean Peninsula based on (a) the full instrumental catalog and (b) a declustered instrumental catalog in which 17 plausible aftershocks are removed. (c) The differences in seismicity densities between the two catalogs $|\Delta C_j|$ are presented. The greatest difference is 0.151. The differences are less than 0.02 in most regions, suggesting high similarity between the two seismicity densities. High-seismicity densities are observed in the northwest and southern inland regions, and the western and southeastern offshore regions. On the other hand, relatively low seismicities are observed in the southern and central inland regions, and northeastern offshore region.

damage rather than to the other cities. A distance-dependent weighting function, probability density function F_{ij}, is introduced in equation (1) to reflect the proximity of actual epicenters to the places with the greatest damage.

Large weights are given to locations close to the cities with the greatest damage, whereas small weights are given to regions located away from the most damaged cities. Thus, the chance of being selected as an epicenter decreases with distance. The decay rate with distance is controlled by K in equation (6). The decay rate increases with K. When a high K is applied, large weights are given to regions at near distances (Fig. 6). On the other hand, comparable weights are calculated between near and far distances when a low K is applied. Parameter K is set so that the spatial distribution of determined historical epicenters resembles the instrumental seismicity density. A large K can be applicable to cases with spatially dense distribution of cities, in which the epicenters are determined to be near the cities with the greatest damage.

The maximum distance $d_{\max}$ is determined considering the geographical distribution of major cities in which local administrative and military centers (Bu, Daedohobu, and Mok) are located (National Institute of Korean History, 2007; Fig. 7). The average distance between adjacent cities d_{avg} is 43.8 km. The maximum distance $d_{\max}$ for inland events may not exceed the distances between adjacent cities because the cities located closer to epicenters may have greater damage. Thus, the average distance among adjacent cities d_{avg} can be applicable for maximum distance in the analysis of both inland and offshore earthquakes.

Epicentral Intensity and Magnitude

The magnitude is determined using the reported intensities I and epicentral distances from equation (10). The epicenters are set to be determined at locations with distances equal to or less than $d_{\max}$ (43.8 km) from the most damaged places in the historical literatures. Thus, the intensity differences between the determined epicenters and the reported most damaged places ($I_0 - I$) are equal to or less than 2.47 (Fig. 2b). Epicentral seismic intensities of 3.0–8.5 correspond to magnitudes of 2.87–7.49 from equation (10).

Determination of K and P_c

For a plausible epicentral location of a historical earthquake, a cell with normalized probabilities P_{ij}^n greater than a prescribed value P_c is randomly selected. Here, the probabilities P_{ij}^n are subject to change with the adopted decay-rate parameter K in equation (6). The decay-rate parameter K should be adjusted so that the probabilities P_{ij}^n can be greater than P_c up to a distance of $d_{\max}$ (43.8 km). The prescribed value P_c controls the pool of potential locations of epicenters. Both the decay parameter K and prescribed value P_c are important for the reasonable determination of historical epicenters.

The epicenters and magnitudes of historical events are examined for implementation of various sets of P_c and K. The prescribed value P_c is set to 0.1, and the decay-rate parameter K varies from 0.01 to 0.09 with an increment of 0.04 (Fig. 8). For small K values, the weighting factors are determined to be comparable with increasing distance (Fig. 8a). Thus, the probabilities are mainly influenced by the instrumental seismicity density, yielding similarity in spatial distribution of epicenters between historical and instrumental seismicity (Fig. 1a). On the other hand, for large K, epicenters are determined at locations close to the cities with the most severe damage (Fig. 8c). This is because a large K causes rapid decrease in probability with distance. Thus, only locations near the places with the most severe damage are found to have probabilities greater than the prescribed value P_c.

We now set P_c to be 0.1, 0.4, and 0.7, for K of 0.005 and 0.65 (Fig. 9). The number of candidate cells for epicenters typically decreases with increasing P_c. Thus, the implementation of a large P_c allows us to determine epicentral locations among limited numbers of candidate cells. The determination of epicenters can be biased in regions with sparse distribution of major cities for implementation of a large P_c

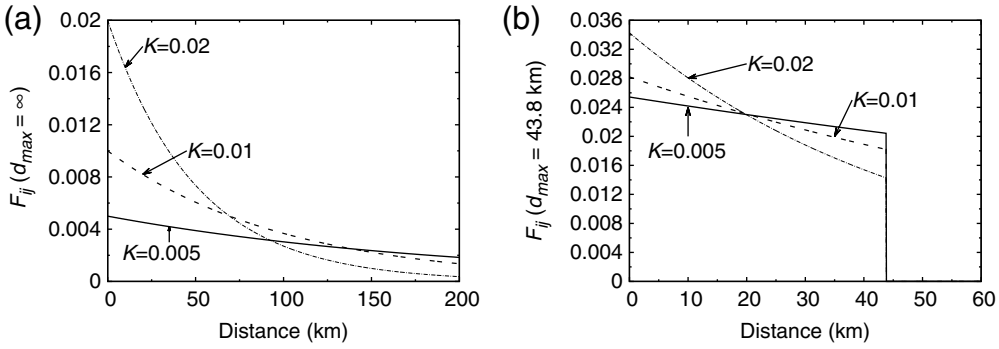

Figure 6. Distance-dependent weighting function F_{ij} with (a) $d_{\max} = \infty$ and (b) $d_{\max} = d_{\text{avg}}$ (i.e., 43.8 km) for various K values (0.005, 0.01, and 0.02). The horizontal axis is the distance in kilometer between the recorded most damaged location of the ith event and the location of the jth cell. The decay rate of F_{ij} increases with K. For a large K ($K = 0.02$), the distance-dependent weighting function has high probability at short distances. For a small K ($K = 0.005$), the distance-dependent weights at different distances are determined to be comparable. For inland and most coastal earthquakes, d_{avg} is used for $d_{\max}$.

because the probabilities P_{ij} are estimated high naturally at locations near the cities with the most severe damage. As small numbers of candidate locations are included in the pools, epicenters can be determined around particular positions. On the other hand, the implementation of a small P_c expands the pool of candidate cells, and increases the chances for far-distant cells to be selected as epicentral locations. The determined epicentral locations are typically clustered around high instrumental seismicity density regions when a small K and a large P_c are applied (e.g., $K = 0.005$, $P_c = 0.7$; Fig. 9c).

The spatial distribution of epicenters appears to be close to the instrumental seismicity for implementation of small K and P_c, whereas the epicenters are determined at regions around the cities with the most severe damage for implementation of a large K with arbitrary P_c (Fig. 9d–f). The observations suggest that a small P_c with a proper decay-rate parameter K may be needed to reasonably study historical seismicity.

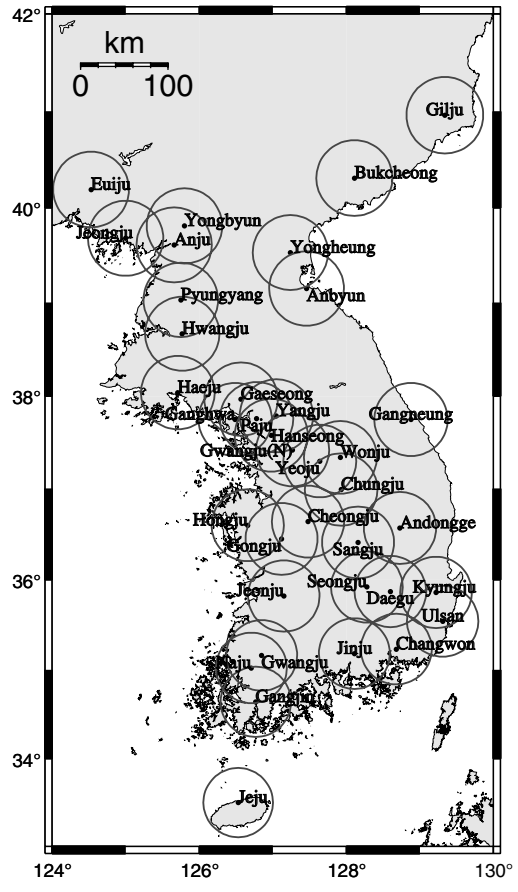

Figure 7. Map of major cities (Bu, Daedohobu, and Mok) of the Choseon dynasty. Circles with a radius of $d_{avg} = 43.8$ km are plotted around the cities. The number of major cities is 37. The cities are distributed densely on the southern peninsula, but relatively sparsely on the northern peninsula. The spatial distribution of the major cities is similar to that of reported locations with seismic damage (Fig. 1b).

We determine the decay-rate parameter K by examining the spatial distribution of historical epicenters. To determine K, we consider a fictitious situation in which two towns are separated by 14 km in a region (Fig. 10a). The epicentral locations of 10,000 events are calculated for a case in which one city has greater damage than does the other city. The epicentral locations of the events are selected from a common pool of candidate cells. Similarly, a set of epicentral locations of events is calculated for the inverse case that the other city has greater damage. Because the epicenters are determined randomly from the pools of candidate locations, the selection probability of a certain location in 10,000 epicenters should resemble the background instrumental seismicity density.

The numbers of events located in the overlapping region between the two cases are compared. The comparison allows us to calculate the similarity of seismicity densities between the two cases. The comparison is conducted for various K values of 0.005–0.085 with an increment of 0.005 (Fig. 10b). Similarities of 0.9 or greater are observed at K of 0.04 or less. The similarities decrease with K in the range of $K > 0.04$. The low similarities mean that the determined epicentral locations agree poorly with the instrumental seismicity, which violates the theory.

From the analysis, we find that the optimum decay-rate parameter K is 0.04, which satisfies the assumptions in the theory and the nature of the probability density function. Also, we set P_c to be 0.1, which is sufficiently small to generate large pools of candidate cells for epicentral locations. The small P_c allows stable analysis with little sensitivity to small variations in input parameters for the calculation of probability P_{ij}.

Validation Test

Repeated occurrence of earthquakes in time and space has been widely reported (e.g., Nadeau *et al.*, 1995; Wiens and Snider, 2001; Schaff and Richards, 2004). Earthquakes occur in weak media, and keep the media weak. Thus, it is often observed that earthquakes are clustered in certain weak zones and structures (e.g., Liu and Zoback, 1997; Gangopadhyay and Talwani, 2003; Choi *et al.*, 2012; Hong and Choi, 2012), and a long-period correlation between instrumental and historical earthquakes is well observed (e.g., Musson, 1998).

We verify the idea that the spatial distribution of long-term seismicity can be represented by that of short-term instrumental seismicity density. Instrumental seismicity records for California during 1973–2012 are collected from the National Earthquake Information Center (NEIC). The catalog is composed of 22,659 local and regional earthquakes with magnitudes of 2.0–7.0 and focal depths of 0–71 km. Also, event information of 478 major earthquakes with magnitudes of 5.0–8.2 in California during 1906–2012 is collected from the International Seismological Center (ISC).

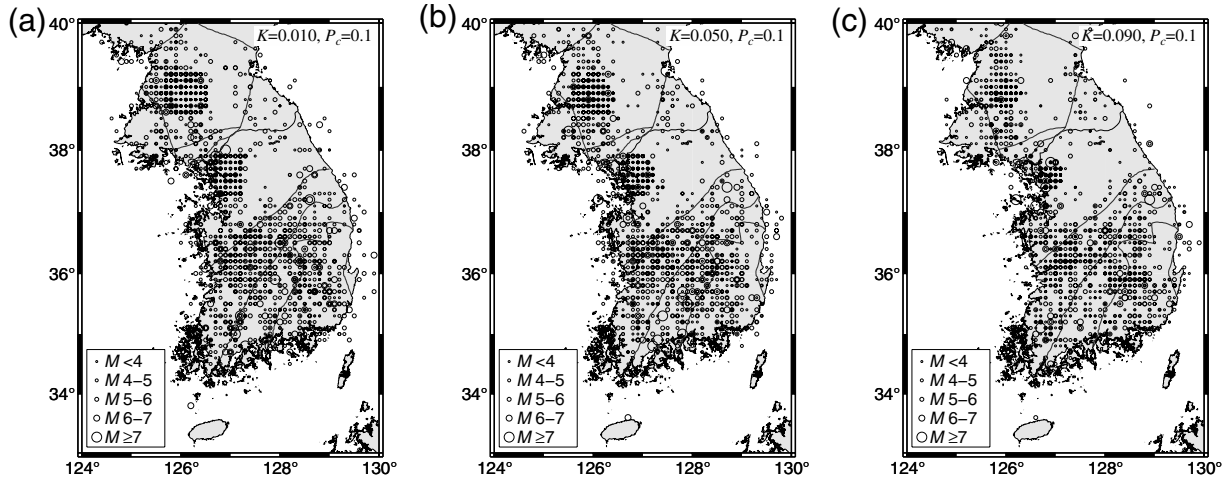

Figure 8. Epicenters and magnitudes of historical earthquakes determined from analyses with $P_c = 0.1$ for (a) $K = 0.01$, (b) 0.04, and (c) 0.09. The seismicity determined with a small K ($K = 0.01$) is observed to be close to the instrumental seismicity with a wide distribution. On the other hand, the seismicity determined with a large K ($K = 0.09$) displays similarity to the spatial distribution of the most damaged locations. The epicentral locations for a large K appear to be more spatially clustered than those for a small K.

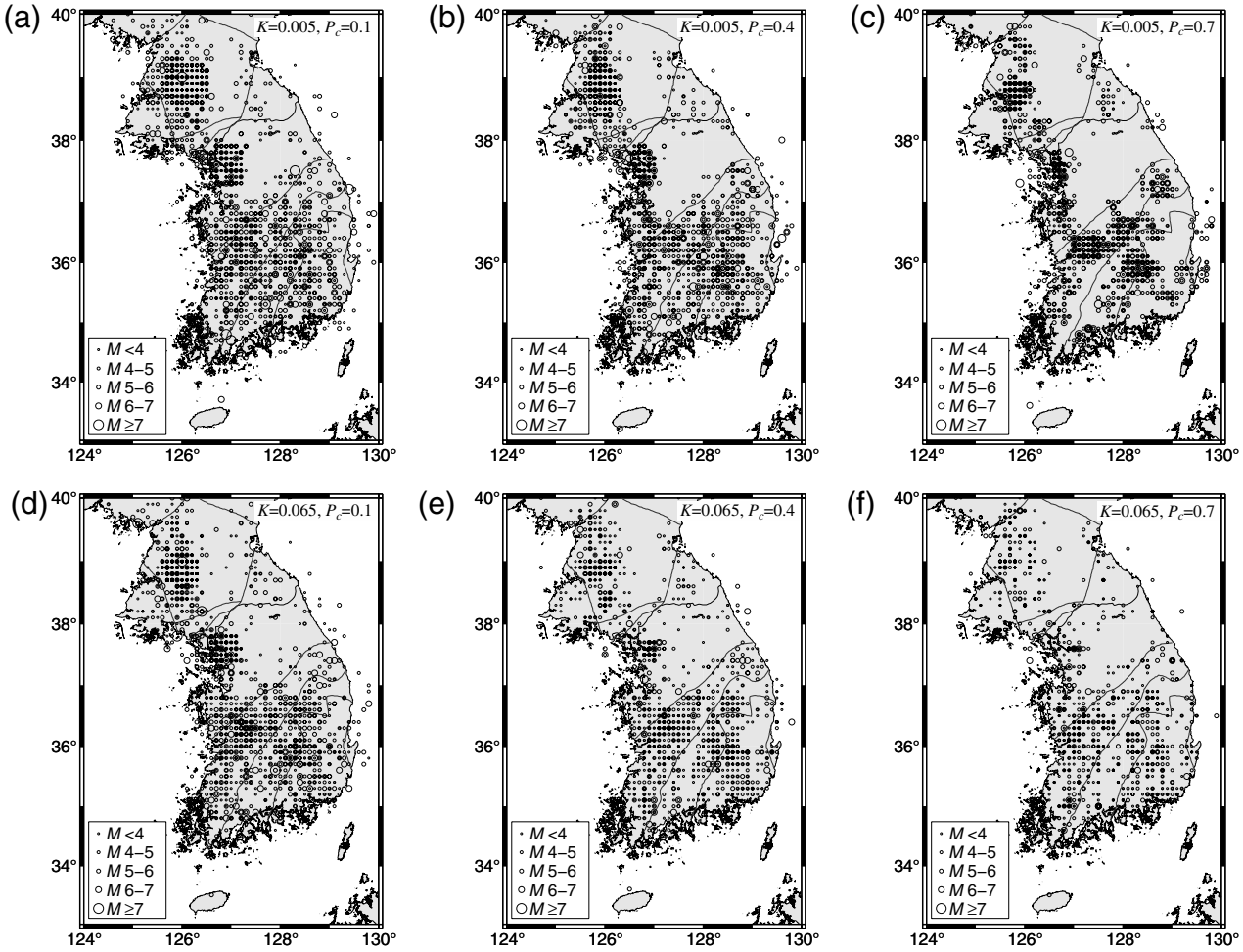

Figure 9. Epicenters and magnitudes of historical earthquakes determined from analyses with (a) K of 0.005 for $P_c = 0.1$, (b) 0.4, and (c) 0.7, and with (d) K of 0.065 for $P_c = 0.1$, (e) 0.4, and (f) 0.7. For a small K ($K = 0.005$), the events become clustered around locations of high instrumental seismicity densities with increase of P_c. On the other hand, for a large K ($K = 0.065$), events are determined to be near the reported most damaged locations with increasing P_c.

Table 2
Source Information and Reported Maximum Intensities of Three Earthquakes (E1, E2, and E3) in California

ID	Date (yyyy/mm/dd)	Time (UTC) (hh:mm:ss)	Latitude (°N)	Longitude (°W)	Magnitude (M_w)	Maximum Intensity (MMI)
E1	1992/04/25	18:06:04	40.33	124.23	7.2	VIII
E2	1983/05/03	00:42:00	36.23	120.32	6.5	VIII
E3	1991/06/28	14:43:54	34.26	118.00	5.7	VIII

Each event was well felt. The seismic intensities are given in the modified Mercalli intensity (MMI) scale.

The instrumental seismicity densities in California are calculated for three different time periods of 5, 20, and 40 years (Fig. 11). The epicenters of the major earthquakes during 1906–2012 are plotted over the seismicity density maps for comparison. The seismicity densities appear to be very similar among the different time periods. The epicenters of major earthquakes correlate well with high-seismicity density regions, which is evident even in the 5 year long seismicity density map (Fig. 11a). The observation supports the idea that the spatial distribution of short-term seismicity may represent that of long-term seismicity.

To test the method of determining epicenters based on intensity reports, we collect seismic intensity data for three earthquakes in California from the U.S. Geological Survey (USGS; Table 2). The method proposed in this paper is applied to the seismic intensity data, and the probable locations of the events are determined from the seismic intensity data and instrumental seismicity density. The hypocentral parameters of the instrumentally recorded events are known. The probable locations of events are compared with the instrumentally determined epicenters (Fig. 12). The instrumentally determined epicentral locations belong to the pools of probable locations in all cases. The observation suggests that the proposed method infers the epicenters reasonably using the seismic intensity data and reference seismicity densities.

Analysis of Historical Seismicity

A set of reference epicenters of historical events are calculated with $K = 0.04$ and $P_c = 0.1$. We calculate 100 sets of epicenters with different random-number seeds. Three representative sets are presented in Figure 13. Some changes in the locations and magnitudes of particular events are observed. However, the overall features of historical seismicity are found to be nearly consistent among different sets. The magnitudes of historical events are found to be around 2.87–7.45. The maximum magnitude is greater than the observed instrumental maximum magnitude by about 2.15 in magnitude units.

We find that the epicenters of many coastal events are determined to be in offshore regions. Inland events are found to be clustered around high instrumental seismicity regions. We find relatively low seismicity on the central Korean Peninsula. However, historical earthquakes are found to be clustered around the Seoul metropolitan region (Hanseong in Choseon dynasty) and suburbs. These earthquakes may be associated with historical reports on seismic damage in the capital city, Seoul. The observation suggests that seismic damage in the capital city may be caused by moderate size or large events at local or near-regional distances.

The Gutenberg–Richter b value of historical events is determined to be 0.73 on average with standard deviation

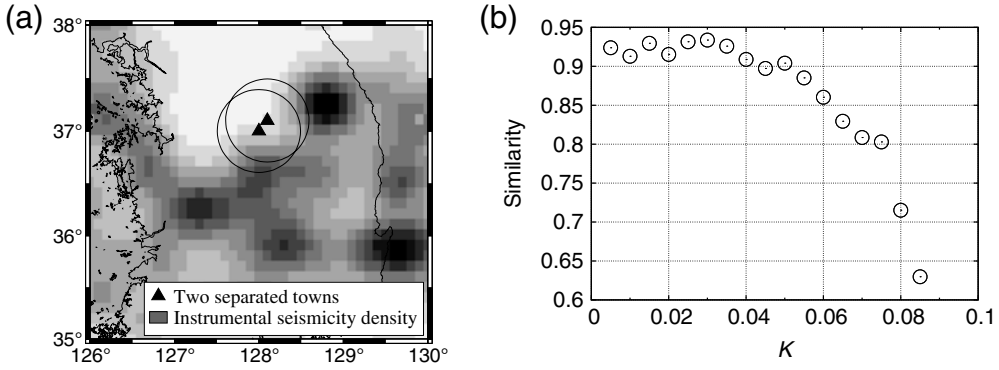

Figure 10. Synthetic test for the determination of optimal K value: (a) map of geometry of two imaginary towns (closed triangles) on the central peninsula, and (b) variation of similarities with change of K. The two towns are separated by 14 km. The instrumental seismicity density is presented on the map, and two circles with a radius of d_{avg} are drawn around the cities. Each town is assumed to be the most damaged place for a certain event, and the epicentral locations are determined by 10,000 random realizations. The population of determined epicenters is supposed to be proportional to the instrumental seismicity density. The populations of the determined epicenters in the region shared by two circles are compared between two results. The similarity of the populations in the shared region is consistently as high as 0.9 for K equal to or less than 0.04, and starts to decrease with increasing K at $K > 0.04$.

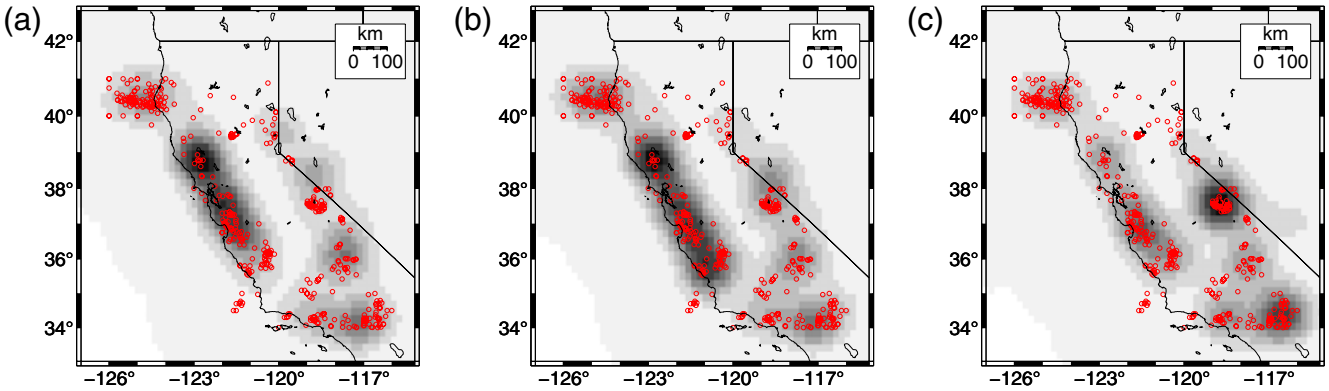

Figure 11. Gray clouds, seismicity densities of California that are calculated based on earthquake catalogs during (a) 2008–2012, (b) 2003–2012, and (c) 1973–2012. Open circles, major earthquakes with magnitudes greater than or equal to 5.0 since 1906. The seismicity density maps are observed to be very similar among different time periods. The epicenters of major earthquakes overlap well with high-seismicity regions. The color version of this figure is available only in the electronic edition.

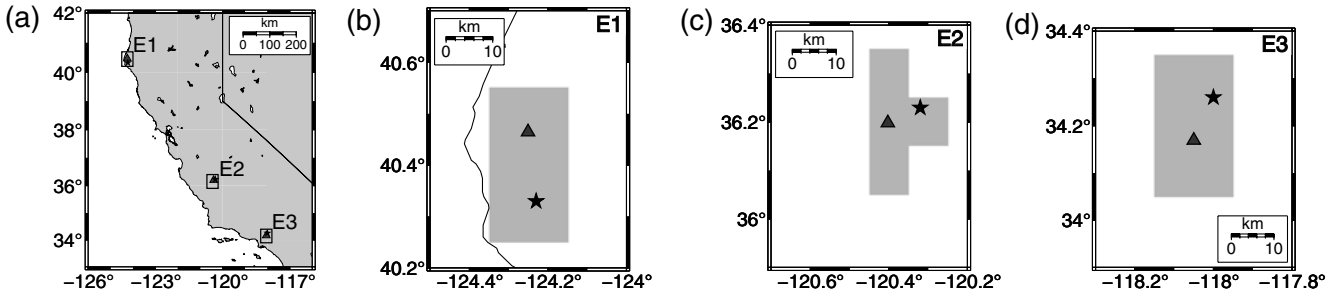

Figure 12. Probabilistic locationing of three earthquakes with reported seismic intensities in California using the method introduced in this paper. (a) Map of stars, instrumentally determined epicenters and triangles, locations of the greatest intensities. Gray areas, probable locations of events determined by the proposed method for events (b) E1, (c) E2, and (d) E3. The pools of candidate locations include the instrumentally determined epicenters in all cases.

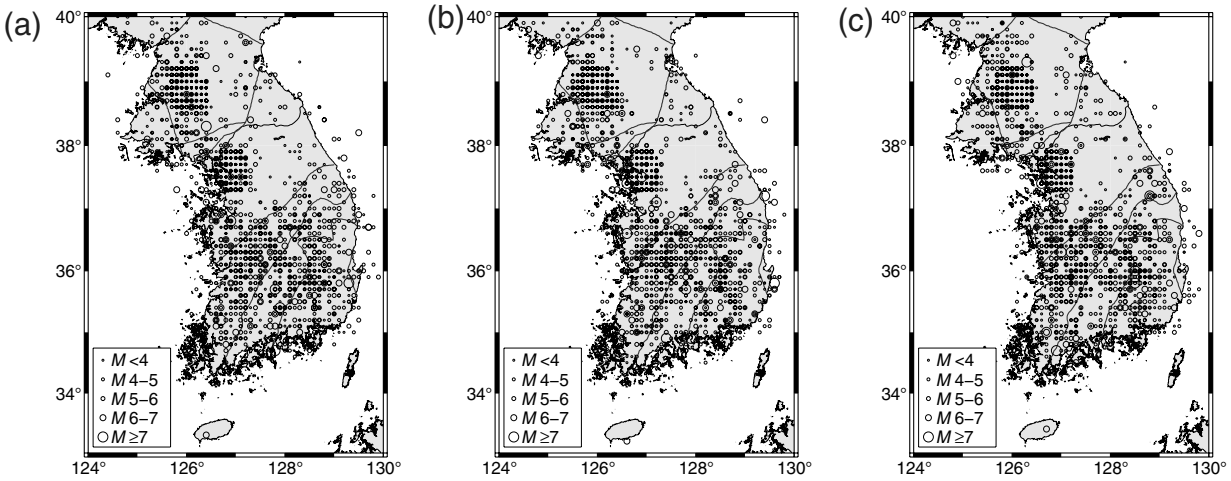

Figure 13. Three sets of epicenters and magnitudes of historical earthquakes determined from analyses with $K = 0.04$ and $P_c = 0.1$. The three sets presented are out of 100 sets of results based on different random seeds. Epicentral locations and magnitudes of individual events are observed to change by random seed. The overall features of seismicity are found to be consistent.

of 0.02 for M_{min} of 5.0, supporting the consistency in overall features among different sets (Fig. 14). The Gutenberg–Richter b value of historical seismicity is observed to be smaller than that of the instrumental seismicity, which is given as 0.81 (Fig. 3b). The difference may be partly associated with possible missing records for some historical events. Also, the observation suggests that the short history of instrumental monitoring may be insufficient for inference of earthquake-occurrence frequencies.

Discussion and Conclusions

Historical earthquake records are a valuable complement to insufficient instrumental seismicity data. Seismic-hazard analyses combining both historical and instrumental earthquake records may be useful, particularly for low-seismicity regions such as the Korean Peninsula. It is known that at least 48 devastating earthquakes causing seismic intensities greater than VIII occurred in this area historically. Among these devastating earthquakes, 37 events were recorded during the Choseon dynasty in 1392–1904. However, earthquake records in the historical literature mainly focus on descriptions of seismic damage with a lack of information on actual magnitudes and epicentral locations. To solve this problem, we proposed a probabilistic location method to determine the epicenters of historical events.

The probability of potential location is calculated based on instrumental seismicity and a distance-dependent weighting factor. The epicenters of historical earthquakes are determined from a pool of probable locations. The magnitudes of historical events are evaluated for the determined epicenters. The proposed method was tested with intensity reports for earthquakes with known source parameters in California. It was observed that the pools of candidate locations include the instrumentally determined epicenters well in all cases, verifying the algorithm of the method. Also, the consistent seismicity properties of historical earthquakes among 100 sets suggest the stability of the method. Also, this observation supports the applicability of the method to probabilistic analysis of historical seismicity analysis.

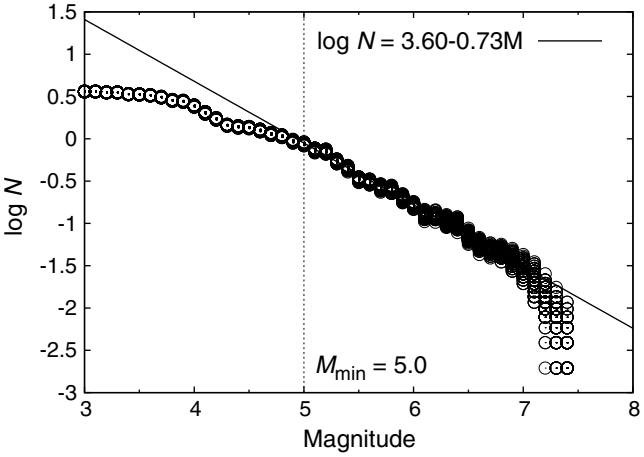

Figure 14. Calculation of Gutenberg–Richter magnitude–frequency relationship for the historical seismicity based on 100 sets of magnitude data from analyses with $K = 0.04$ and $P_c = 0.1$. The magnitude datasets are found to be consistent with each other. The minimum magnitude (M_{min}) is determined to be 5.0, which indicates the threshold magnitude for record completeness. The b value is determined to be 0.73 with standard deviation of 0.02.

From the analysis of historical earthquakes, we find several clustered seismicity regions including the northwestern peninsula (Ongjin basin, Pyeongnam basin), the western region around the Seoul metropolitan region, the southeast offshore region beneath the East Sea, and the southern peninsula (Okcheon fold belt, Yeongnam massif, Gyeongsang basin). These historical seismicity features are generally consistent with the instrumental seismicity features. In particular, events with magnitudes greater than 6.0 are observed around the regions with high instrumental seismicity. The maximum magnitude of the historical events is observed to be 7.45 ± 0.04 from 100 sets of results. The observed maximum magnitude is greater than the instrumentally observed maximum magnitude by 2.15 magnitude units. Further, the Gutenberg–Richter b value of historical seismicity is estimated to be 0.73 ± 0.02, which is smaller than that of instrumental seismicity (0.81).

The probabilistic analysis of historical seismicity allows us to reasonably determine the spatial density of historical seismicity, maximum magnitude, and Gutenberg–Richter b value. In addition, the method enables us to infer the potential seismic hazard of earthquakes with long recurrence intervals, which is important information for seismic-hazard mitigation.

Data and Resources

The seismic source information of instrumental seismicity was collected from the Korea Meteorological Administration (KMA) using www.kma.go.kr/mini/earthquake/main.jsp (last accessed August 2012). The source information for earthquakes in California was collected from the National Earthquake Information Center (NEIC) and International Seismological Center (ISC) using www.earthquake.usgs.gov/regional/neic and www.isc.ac.uk/iscbulletin (last accessed February 2013). Seismic intensity data for earthquakes in California were collected from the U.S. Geological Survey (USGS) using www.earthquake.usgs.gov/earthquakes/dyfi (last accessed February 2013).

Acknowledgments

We are grateful to Yoon-Oh Choi at Yonsei University who gave us valuable comments about the geography of historical cities and historical literature. We thank Mark Williamson Stirling and two anonymous reviewers for their constructive review comments that improved the presentation of this paper. This work was supported by project Earthquake monitoring at nuclear power plant (NPP) site of the Korean Institute of Nuclear Safety, and by the Korea Meteorological Administration Research and Development Program under Grant CATER 2012-8050.

References

Albarello, D., and M. Mucciarelli (2002). Seismic hazard estimates using ill-defined macroseismic data at site, *Pure Appl. Geophys.* **159,** 1289–1304.

Ambraseys, N. N. (1971). Value of historical records of earthquakes, *Nature* **232,** 375–379.

Ares, A. F., and A. Fatehi (2013). Development of probabilistic seismic hazard analysis for international sites, challenges and guidelines, *Nucl. Eng. Des.* **259,** 222–229.

Bakun, W. H., and C. M. Wentworth (1997). Estimating earthquake location and magnitude from seismic intensity data, *Bull. Seismol. Soc. Am.* **87,** 1502–1521.

Bath, M. (1965). Lateral inhomogeneities of the upper mantle, *Tectonophysics* **2,** 483–514.

Chang, S.-J., and C.-E. Baag (2006). Crustal structure in southern Korea from joint analysis of regional broadband waveforms and travel times, *Bull. Seismol. Soc. Am.* **96,** 856–870.

Choi, H., T.-K. Hong, X. He, and C.-E. Baag (2012). Seismic evidence for reverse activation of a paleo-rifting system in the East sea (Sea of Japan), *Tectonophysics* **572–573,** 123–133.

Chough, S. K., S.-T. Kwon, J.-H. Ree, and D. K. Choi (2000). Tectonic and sedimentary evolution of the Korean peninsula: A review and new view, *Earth Sci. Rev.* **52,** 175–235.

Degasperi, C., D. Slejko, A. Rebez, and M. Cergol (1991). Earthquakes felt in Trieste from the middle ages to the 18th century, *Tectonophysics* **193,** 53–63.

Engdahl, E. R., and A. Villasenor (2002). Global Seismicity: 1900–1999, in *International Handbook of Earthquake and Engineering Seismology, Part A*, W. H. K. Lee, H. Kanamori, P. C. Jenning, and C. Kisslinger (Editors), Chapter 41, Academic Press, New York, 665–690.

Ernst, W. G., T. Tsujimori, R. Zhang, and J. G. Liou (2007). Permo-Triassic collision, subduction-zone metamorphism, and tectonic exhumation along the east Asian continental margin, *Annu. Rev. Earth Planet. Sci.* **35,** 73–110.

Frankel, A. (1995). Mapping seismic hazard in the central and eastern United States, *Seismol. Res. Lett.* **66,** 8–21.

Gangopadhyay, A., and P. Talwani (2003). Symptomatic features of intraplate earthquakes, *Seismol. Res. Lett.* **74,** 863–883.

Geller, R. J. (2011). Shake-up time for Japanese seismology, *Nature* **472,** 407–409.

Goto, K. (2011). Geological overview of the 2011 Tohoku-Oki tsunami in Japan, *AGU Fall Meeting 2011*, Abstract NH53B-08.

Helmstetter, A., and D. Sornette (2003). Båth's law derived from the Gutenberg–Richter law and from aftershock properties, *Geophys. Res. Lett.* **30,** 2069–2072, doi: 10.1029/2003GL018186.

Hirata, N., H. Tokuyama, and T. W. Chung (1989). An anomalously thick layering of the crust of the Yamato basin, southeastern Sea of Japan: The final stage of back-arc spreading, *Tectonophysics* **165,** 303–314.

Hong, T.-K. (2010). *Lg* attenuation in a region with both continental and oceanic environments, *Bull. Seismol. Soc. Am.* **100,** 851–858.

Hong, T.-K., and H. Choi (2012). Seismological constraints on the collision belt between the North and South China blocks in the Yellow Sea, *Tectonophysics* **570–571,** 102–113.

Hong, T.-K., and T.-S. Kang (2009). *Pn* traveltime tomography of the paleo-continental-collision and rifting zone around Korea and Japan, *Bull. Seismol. Soc. Am.* **99,** 416–421.

Hong, T.-K., C.-E. Baag, H. Choi, and D.-H. Sheen (2008). Regional seismic observations of the 9 October 2006 underground nuclear explosion in North Korea and the influence of crustal structure on regional phases, *J. Geophys. Res.* **113,** B03305, doi: 10.1029/2007JB004950.

Jolivet, L., K. Tamaki, and M. Fournier (1994). Japan Sea, opening history and mechanism: A synthesis, *J. Geophys. Res.* **99,** 22,237–22,259.

Kagan, Y. Y., and D. D. Jackson (2000). Probabilistic forecasting of earthquakes, *Geophys. J. Int.* **143,** 438–453.

Kijko, A., and G. Graham (1998). Parametric-historic procedure for probabilistic seismic hazard analysis part I: Estimation of maximum regional magnitude m_{max}, *Pure Appl. Geophys.* **152,** 413–442.

Kim, H.-J., S.-J. Han, G. H. Lee, and S. Huh (1998). Seismic study of the Ulleung Basin crust and its implications for the opening of the East Sea (Japan Sea), *Mar. Geophys. Res.* **20,** 219–237.

Kim, S. K. (2012). Korean historical and instrumental earthquake catalogues, in *International Workshop on KHNP SSHAC Project*, Gyeongju, South Korea, 11–13 October 2012.

Klugel, J.-U. (2005). Problems in the application of the SSHAC probability methods for assessing earthquake hazards at Swiss nuclear power plants, *Eng. Geol.* **78,** 285–307.

Koketsu, K. (2012). Seismological and geodetic aspect of the 2011 Tohoku earthquake and great east Japan earthquake disaster, in *Proc. of the International Symposium on Engineering Lessons Learned from the 2011 Great East Japan Earthquake*, Tokyo, Japan, 1–4 March 2012.

Koravos, G. C., I. G. Main, T. M. Tsapanos, and R. M. W. Musson (2003). Maximum earthquake magnitudes in the Aegean area constrained by tectonic moment release rates, *Geophys. J. Int.* **152,** 94–112.

Kulinich, R. G., and M. G. Valitov (2011). Thicknesses and types of the crust beneath the Sea of Japan inferred from marine and satellite gravimetric investigations, *Russ. J. Pacif. Geol.* **5,** 481–491.

Lee, K., and J.-K. Kim (2002). Intensity attenuation in the Sino–Korean craton, *Bull. Seismol. Soc. Am.* **92,** 783–793.

Lee, K., and J. H. Lee (2003). Short note: Magnitude–intensity relation for earthquakes in the Sino–Korean craton, *Seismol. Res. Lett.* **74,** 350–352.

Lee, K., and W.-S. Yang (2006). Historical seismicity of Korea, *Bull. Seismol. Soc. Am.* **96,** no. 3, 846–855.

Lee, K., N. S. Chung, and T. W. Chung (2003). Earthquakes in Korea from 1905 to 1945, *Bull. Seismol. Soc. Am.* **93,** 2131–2145.

Lee, D. S., K. J. Ryu, and G. H. Kim (1983). Geotectonic interpretation of Choogaryong rift valley, Korea, *Jijirhag Hoiji/J. Geol. Soc. Korea* **19,** 19–38 (in Korean).

Lee, W. H. K., F. T. Wu, and C. Jacobsen (1976). A catalog of historical earthquakes in China compiled from recent Chinese publication, *Bull. Seismol. Soc. Am.* **66,** 2003–2016.

Liu, L., and M. D. Zoback (1997). Lithospheric strength and intraplate seismicity in New Madrid seismic zone, *Tectonics* **16,** 585–595.

Miyazawa, M., and J. Mori (2009). Test of seismic hazard map from 500 years of recorded intensity data in Japan, *Bull. Seismol. Soc. Am.* **99,** 3140–3149.

Mueller, C. S. (2010). The influence of maximum magnitude on seismic-hazard estimates in the central and eastern United States, *Bull. Seismol. Soc. Am.* **100,** 699–711.

Musson, R. M. W. (1998). Inference and assumption in historical seismology, *Surv. Geophys.* **19,** 189–203.

Nadeau, R. M., W. Foxall, and T. V. McEvilly (1995). Clustering and periodic recurrence of microearthquakes on the San Andreas fault at Parkfield, California, *Science* **27,** 503–507.

National Institute of Korean History (2007). *The Korean History*, Vol. 2, Kyohaksa, Seoul, 435 pp. (in Korean).

Ogata, Y., and K. Katsura (1993). Analysis of temporal and spatial heterogeneity of magnitude frequency distribution inferred from earthquake catalogs, *Geophys. J. Int.* **113,** 727–738.

Oh, C. W. (2006). A new concept on tectonic correlation between Korea, China, and Japan: Histories from the late Proterozoic to Cretaceous, *Gondwana Res.* **9,** 47–61.

Okal, E. A., and J. R. Sweet (2007). Frequency–size distributions for intraplate earthquakes, *Spec. Pap. Geol. Soc. Am.* **425,** 59–71.

Poirier, J. P., and M. A. Taher (1980). Historical seismicity in the near and Middle East, North Africa, and Spain from Arabic documents (VIIth–XVIIIth century), *Bull. Seismol. Soc. Am.* **70,** 2185–2201.

Rao, B. R., and P. S. Rao (1984). Historical seismicity of Peninsula India, *Bull. Seismol. Soc. Am.* **74,** 2519–2533.

Rubbia, G. (2004). A review of intensity data banks online, *Ann. Geophys.* **47,** 873–884.

Ryu, S., M. Oka, K. Yagi, T. Sakuyama, and T. Itaya (2011). K-Ar ages of the Quaternary basalts in the Jeongok area, the central part of Korean peninsula, *Geosci. J.* **15,** 1–8.

Sato, T., T. Sato, M. Shinohara, R. Hino, M. Nishino, and T. Kanazawa (2006). P-wave velocity structure of the margin of the southeastern Tsushima basin in the Japan Sea using ocean bottom seismometers and airguns, *Tectonophysics* **3–4,** 159–171.

Schaff, D. P., and P. G. Richards (2004). Repeating seismic events in China, *Science* **303,** 1176–1178.

Seo, J.-M., I.-K. Choi, and H.-M. Rhee (2010). A study of the historical earthquake catalog and Gutenberg–Richter parameter values of the Korean Peninsula, *Nucl. Eng. Tech.* **42,** 55–64.

Sheen, D.-H., and J. S. Shin (2010). Earthquake detection thresholds of broadband seismic networks in South Korea considering background seismic noise levels, *J. Geol. Soc. Korea* **46,** 31–38 (in Korean).

Shibuya, H., K. D. Min, Y. S. Lee, S. Sasajima, and S. Nishimura (1985). Some paleomagnetic measurements in Korean Peninsula, in *Physical Geology of Central and Southern Part of Korea*, S. Nishimura and K. D. Min (Editors), Kyoto Univ., Kyoto, 41–83.

Thingbaijam, K. K. S., and S. K. Nath (2008). Estimation of maximum earthquakes in northeast India, *Pure Appl. Geophys.* **165,** 889–901.

Uhrhammer, R. (1986). Characteristics of northern and central California seismicity, *Earthq. Notes* **57,** 21.

Usami, T. (1979). Study of historical earthquakes on Japan, *Bull. Earthq. Res. Inst. Tokyo Univ.* **54,** 399–439.

Wada, Y. (1912). A survey of Korean ancient and recent earthquakes, report of the study of Korean ancient observations, *Meteorological Observatory of the Government General of Korea*, 79–105 (in Japanese).

Wiemer, S., and M. Wyss (2000). Minimum magnitude of completeness in earthquake catalogs: Examples from Alaska, the Western United States, and Japan, *Bull. Seismol. Soc. Am.* **90,** 859–869.

Wiens, D. A., and N. O. Snider (2001). Repeating deep earthquakes: Evidence for fault reactivation of great depth, *Science* **293,** 1463–1466.

Woessner, J., and S. Wiemer (2005). Assessing the quality of earthquake catalogues: Estimating the magnitude of completeness and its uncertainty, *Bull. Seismol. Soc. Am.* **95,** 684–738.

Won, C. K., Y. K. Kim, and M. W. Lee (1990). The study on the geochmistry of Choogaryong alkali basalt, *J. Geol. Soc. Korea* **26,** 70–81 (in Korean).

Yonsei University
Department of Earth System Sciences
50 Yonsei-ro, Seodaemun-gu
Seoul 120-749, South Korea
tkhong@yonsei.ac.kr

Manuscript received 25 October 2012